

Water-Gas Shift Reaction in Ceramic-Carbonate Dual-Phase Membrane Reactor at High Temperatures and Pressures

Oscar Ovalle-Encinia and Jerry Y.S. Lin *

School for Matter, Transport and Energy (SEMTE), Arizona State University,
Tempe, AZ 85287

Abstract

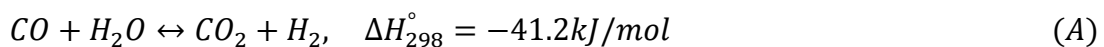
Water-gas-shift (WGS) reaction is a critical step in integrated gasification combined cycles (IGCC) power plants with CO₂ capture. Membrane reactors made with a CO₂-permselective ceramic-carbonate dual-phase (CCDP) membrane offers the potential to enhance hydrogen yield with simultaneous CO₂ capture for WGS reaction. The present work studies operation of WGS reaction in a tubular membrane reactor made of samarium-doped ceria infiltrated with lithium/sodium molten carbonate mixture. The WGS reaction was performed in the membrane reactor with and without a high-temperature WGS catalyst at 800-850 °C, feed pressure of 7 bar, the space velocity of 150-3000 h⁻¹, and a feed gas mixture of 45.7/13.1/41.3 mol% CO/CO₂/N₂ with steam to carbon ratio of 4. The results show that the catalyst-free membrane reactor can convert 92% of carbon monoxide into CO₂ and H₂ and recover 29% CO₂ at 850 °C and a space velocity of 150 h⁻¹. However, in the catalyst-free membrane reactor, a significant amount of unwanted carbon deposition is observed. The side reactions can be minimized by reducing the operating pressure and increasing the operating temperature and space velocity, and completely avoided using a high-temperature catalyst at space velocity larger than 500 h⁻¹. The membrane reactor with a WGS catalyst achieves CO conversion of about 85%, above the equilibrium conversion, and 40% CO₂ recovery without carbon deposition at high

temperature and pressure. The membrane remains in the same structure and gas-tightness after the WGS reaction tests.

Keywords: Water gas-shift, carbon deposition, membrane reactor, CO₂ separation, ceramic-carbonate membrane

1. Introduction

Fossil fuel power plants need to reduce anthropogenic carbon dioxide (CO₂) emissions to mitigate global warming and climate change. In this vein, integrated gasification combined cycles (IGCC) power plants can control CO₂ emissions with efficient power generation from coal because the high CO₂ concentration in the precombustion process facilitates its separation/capture, producing high purity hydrogen (H₂) stream [1]. A typical coal-fired IGCC power plant with precombustion CO₂ capture comprises gasification of solid feedstock with oxygen and steam to produce raw syngas, which is a mixture mainly of carbon monoxide (CO) and H₂ [2]. The syngas is cleaned at low temperature, and water-gas shifted (WGS) to produce a stream of CO₂ and H₂ as follows:



The WGS reaction is exothermic, and thus, the thermodynamic equilibrium conversion of CO decreases with increasing temperature. Consequently, two reactors, one at temperatures higher than 400 °C and the other at temperatures lower than 300 °C, are used to promote the kinetic and overcome the equilibrium limitation in order to obtain high CO conversion [3,4]. Then, CO₂ is removed/captured from the WGS product steam by scrubbing with solvents in an acid gas removal unit, followed by the burning of H₂ in a gas turbine to produce heat and then

electricity. The most common industrial CO₂ removal/capture technology is amine absorption which has a high energy penalty [1].

Membrane reactors can improve the conversion of WGS with the separation of CO₂ in the same unit [5,6]. Over the years, membrane reactors made of H₂-permselective membranes have been studied to intensify CO conversion and H₂ production in WGS reactions at temperatures lower than 400 °C. Among the most studied membranes are the palladium (Pd)-based membranes with an iron (Fe)-based catalyst [7–9]. Although these membrane reactors are promising, Pd-alloy membranes still suffer from poor stability under industrial reaction conditions presenting a technological challenge. Other efforts have been devoted to catalytic membrane reactors made of silica [10–12], zeolite (MFI type) [13–15], and ZIF-8 [16] membranes; however, these membranes have low H₂ selectivity, and the membrane reactors could produce a hydrogen stream of less than 90% purity. Also, membrane reactors made of proton-conducting ceramic membranes, i.e., europium doped SrCeO₃, have been reported, but these membranes have very low oxygen permeation fluxes and suffer from stability problems.

Recently, we reported membrane reactors with a CO₂-permselective dense ceramic-carbonate dual-phase (CCDP) membrane for WGS with CO₂ separation in temperatures between 700-950 °C, without using a WGS catalyst, under atmospheric pressure conditions [17]. CCDP membranes are made of an oxygen ionic or mixed ionic-electronic conductor support with pores infiltrated with a eutectic molten carbonate mixture [18–22]. Since CO₂ is transported by CO₃²⁻ ions through the molten-carbonate phase, these membranes provide infinite selectivity for CO₂ over any other chemical species [23,24]. With CO₂ removal the CCDP membrane reactor could achieve CO conversion and CO₂ recovery of 26.1% and 18.7%, respectively, much higher than the conventional fixed bed reactor under identical conditions, and produce essentially pure CO₂

stream [17]. In a modeling study, the performance of WGS in such a membrane reactor can be significantly improved at high feed pressures (e.g., 30 bar) [25].

Our study on WGS in the catalyst-free CCDP membrane reactor was focused on CO conversion and CO₂ capture. It is known that the WGS reaction is accompanied by unwanted side reactions to form carbon (C) and methane (CH₄) in fixed-bed reactors [26–29]. Carbon and CH₄ yields were found to increase with the initial CO₂ amount in the syngas. Both carbon and CH₄ yields decrease as the temperature increases and can be suppressed by increasing the steam to carbon (S/C) ratio [26,27]. Also, high pressure in the reactor can intensify the carbon deposition in catalyzed WGS reaction [29], and nickel-based steam reforming catalyst can also favor C formation due to the dissociation of reactants on the metal surface [28]. However, CH₄ and C yields can be suppressed at high temperatures and high steam to carbon ratios. The introduction of oxygen (O₂) or solid sorbents for CO₂ capture can also minimize CH₄ and C formation. Our recent experimental study [17] shows the promise of using a CO₂ perm-selective CCDP membrane reactor for WGS with simultaneous CO₂ capture but did not address the issue of coking and side reactions. The objective of the present work is to study conditions for WGS reaction with higher CO₂ conversion in CCDP membrane reactor, with focus on understanding effects of side reactions on WGS in the CO₂ permselective membrane reactor.

2. Experimental procedures

2.1. Dense dead-end tubular ceramic-carbonate membrane fabrication

Powders of samarium-doped ceria (SDC) with the chemical formula of Ce_{0.8}Sm_{0.2}O_{2-δ} were synthesized by the citrate method, and dead-end SDC tubes were fabricated by the cold isostatic press (CIP)/sintering method as was reported in our previous publication [24]. Briefly, SDC powders were well packed inside a rubber bag with a stainless-steel rod mold for making the

dead-end tube. The rubber bag was placed inside a metallic vessel with water and pressurized at 1500 bar with a water pressure intensifier setup. The green dead-end tubes were sintered at 1200 °C for 4 hr. The pores of the sintered dead-end tubes were infiltrated with molten carbonate of lithium carbonate (Alpha Aesar 99%) and sodium carbonate (VWR BDH Chemicals 99.5%) at 52:48 molar ratio at 600 °C to form a dense CCDP membrane.

2.2. CCDP membrane characterization

The porous SDC supports, and dense SDC-MC membranes were characterized by X-ray diffraction (XRD) (Bruker AXS D8 device with Cu anode (K_{α} radiation)). The analysis was performed in the 2-theta degree interval of 20 to 100° using a step size of 0.02°. The inner and outer surface and cross-section of membranes were examined by scanning electronic microscopy (SEM) using an Amray-1910 electron microscope. The pore volume fraction (porosity) of the dead-end SDC tubes was measured by the Archimedes method with liquid nitrogen [30]. Helium permeance through the porous SDC supports was measured by a steady-state helium permeation setup at room temperature, and the data was used to calculate the average pore size (\widehat{d}_p) and pore volume fraction to tortuosity ratio ($(\frac{\epsilon}{\tau})_p$) [31]. The gas-tightness of CCDP membranes after carbonate infiltration was confirmed by the room temperature unsteady-state helium permeation method.

2.3. Water-gas shift reaction in CCDP membrane reactor

Experiments on WGS reaction in the membrane reactor without or with a catalyst were performed in a homemade high-temperature/pressure membrane permeation setup, **Figure 1**. The stainless-steel (SS) membrane housing was placed at the center of a tubular furnace. The open end of a CCDP membrane was sealed with a home-designed graphite gasket, and the dead-end side was free-suspended to allow longitudinal thermal expansion/contraction. The gasket was

compressed between a washer and the module head. For the reaction with catalyst, 2.5 gr of high-temperature Co-Mo-Mg(AlO_2)₂ catalyst (SSK-10) (Haldor Topsoe, Lyngby, Denmark) was placed on the outside of the CCDP membrane tube, as shown in **Figure 1**. The module was housed within a tubular furnace, and, to avoid oxidation of the outer surface of the graphite gasket, the permeation module was blanketed with a flow of inert gas of nitrogen. This enabled effective sealing of the SDC-MC membranes at high temperature/pressure for at least 12 hr.

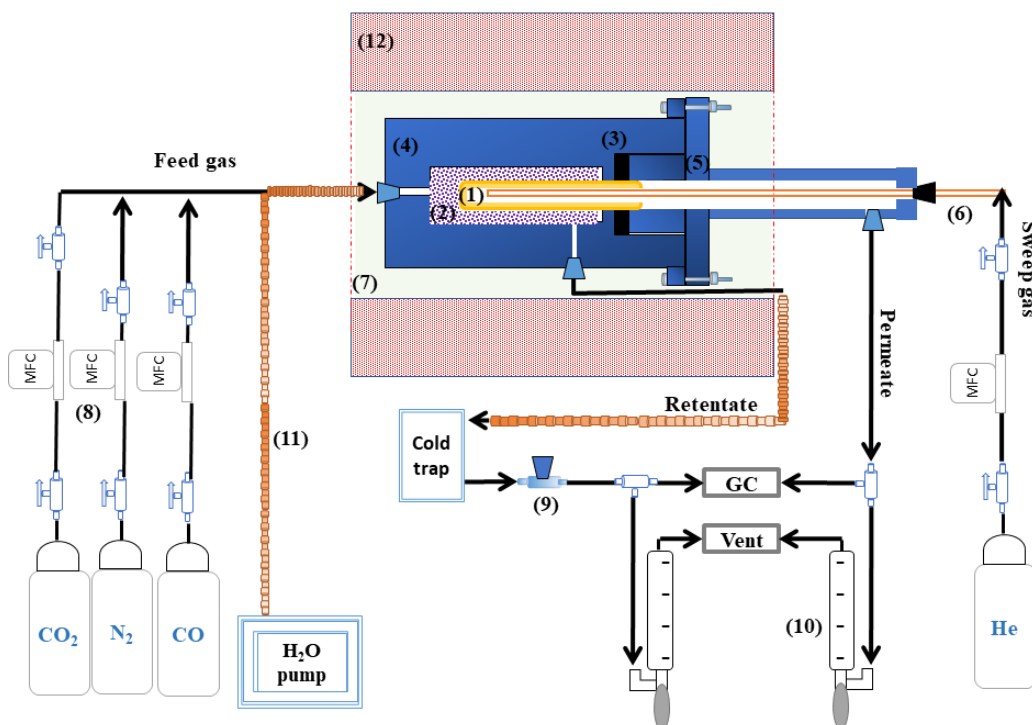


Figure 1. Schematic representation of the setup and permeation cell for high temperatures and pressures WGS reaction tests in CCDP dead-end tubular membranes. (1) CCDP membrane, (2) catalyst, (3) graphite gasket, (4) reaction cell, (5) reaction cell head, (6) alumina tube for sweep gas, (7) inert gas, (8) mass flow controllers, (9) back-pressure regulator, (10) bubble flowmeter, (11) heating-tape, and (12) tubular furnace.

A gas stream of CO/CO₂/N₂/H₂O, formed by mixing a dry gas mixture of 45.7/13.1/41.3 mol% CO/CO₂/N₂ with a controlled amount of steam produced by a pump, is fed as the reactants to the shell side of the membrane tube. The steam to CO (S/C) ratio was controlled at 4, giving the highest CO conversion reported in our previous study [17]. Nitrogen was added to the feed to

simulate raw syngas from the air-blown gasifier. The feed stream of steam was generated by controlling the stream pumping flow rate, and the stainless tubing was heated up with heating tapes at 140 °C to avoid steam condensation. A back-pressure regulator (max. 30.1 atm, Swagelok) was installed after the cold trap on the retentate side to regulate the total feed pressure from 1 to 10 bar. A long thin alumina tube passing through the module head was placed inside the dead-end SDC-MC tubular membrane to introduce sweep gas to the tube side of the membrane to remove the permeate gas. This small alumina tube was sealed outside the furnace with another graphite ferrule. The sweep gas was helium at a total pressure of 1 bar. The membrane tube was heated to the desired temperature at the ramping rate of 1 °C/min. Once a steady-state temperature was reached, the feed pressure was increased to a pre-determined value at the 0.08 bar/min ramping rate.

The composition of retentate and permeate stream was measured by gas chromatography (GC Agilent Technologies 6890N with a TCD detector, Alltech Hayesep DB 100/120 column of 300 1/8" 0.85" SS, and argon as carrier gas). Samples were taken one hour after the change in operating conditions reached the steady-state system. The retentate and permeate flow rates were measured with a bubble flowmeter at the outlets. The compositions and flow rates of the retentate and permeate were used to calculate molar flow rates for various species in the retentate and CO₂ permeation flux through the membrane. The cold trap was installed on the retentate side to condensate water before taking the sample for GC analysis. N₂ concentration in the permeate was neglectable because the SDC-MC membrane is permeable only to CO₂ with less than 1% leakage through the membrane defects (if any) and seals.

The CO conversion (X_{CO}), CO₂ recovery (R_{CO_2}), and carbon balance (B_C) are defined as follows:

$$X_{CO} = \frac{F_{CO}^{feed} - F_{CO}^{retentate}}{F_{CO}^{feed}} \times 100 \quad (1)$$

$$R_{CO_2} = \frac{F_{CO_2}^{retentate}}{F_{CO_2}^{retentate} + F_{CO_2}^{permeate}} \times 100 \quad (2)$$

$$B_C = \frac{F_{CO}^{retentate} + F_{CO_2}^{retentate} + F_{CO_2}^{permeate}}{F_{CO}^{feed} + F_{CO_2}^{feed}} \times 100 \quad (3)$$

where F_i^{feed} , $F_i^{retentate}$, and $F_i^{permeate}$ are the molar flow rates of the feed, retentate, and permeate stream for each gas ($i=CO, CO_2$), in this particular study $F_{CO}^{permeate} = 0$ because the CCDP membrane is CO_2 -permeable only.

3. Results and discussion

Porous SDC tubes prepared by the CIP method followed by sintering at 1200 °C are mechanically quite strong. **Figure 2a** shows that the support is made of sintered SDC particles between 100 and 200 nm, giving an average pore size of about 100 nm. Helium permeance vs. average pressure data for the SDC support exhibits a straight line in **Figure 2b**. The regression of the data gave the slope ($\beta=5.8 \times 10^{-14} \text{ mol}\cdot\text{s}^{-1}\cdot\text{m}^{-2}\cdot\text{Pa}^{-2}$ and y-interception ($\alpha=7.7 \times 10^{-8} \text{ mol}\cdot\text{s}^{-1}\cdot\text{m}^{-2}\cdot\text{Pa}^{-1}$), which were used to calculate average pore diameter, $\widehat{d}_p=190 \text{ nm}$, consistent with SEM observation. The SDC support also has a porosity of 7% and a tortuosity factor of 14.

Figure 2c shows the cross-section of the dense CCDP membrane made by direct infiltration of the pores of the SDC support with the carbonate mixture. The helium permeance after the carbonate infiltration was of the order of $10^{-11} \text{ mol}\cdot\text{s}^{-1}\cdot\text{m}^{-2}\cdot\text{Pa}^{-1}$, which is three orders of magnitude lower than before the infiltration, confirming the membrane is gas-tight. The diffractograms of the outer surface of the SDC support and SDC-carbonate membrane given in **Figure 2d** show a single crystalline structure of the SDC phase for both the SDC support and

SDC-carbonate membrane. The diffraction peaks of the carbonate phase are not observed in the XRD pattern because the intensity of the diffraction peaks is indistinguishable due to the low weight percent of carbonate of 2.2% on the surface of the membrane.

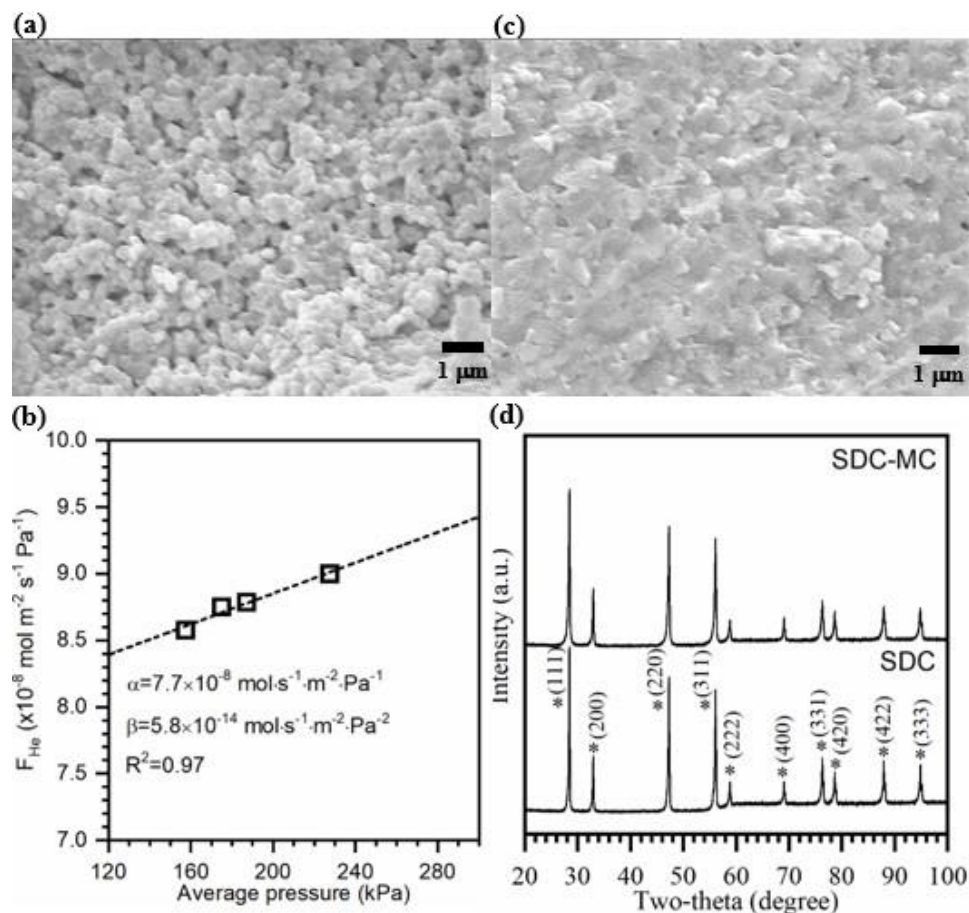


Figure 2. SEM image of the cross-section of (a) SDC support sintered at 1200 °C and (c) SDC-carbonate dense membrane. (b) Helium permeance results as a function of average pressure for SDC support sintered at 1200 °C. (d) XRD patterns of SDC and SDC-carbonate samples. (*) SDC crystalline phase.

The effect of temperature, S/C ratio, and syngas flowrate on WGS reaction performance in CCDP membrane reactor without catalyst was previously investigated by Lin and coworkers [17]. However, the experiments were performed at 1 bar and high space velocities (SV) between 1,619 and 3,055 h^{-1} , resulting in low CO conversion (<30%). In the present work, experiments were performed at lower SV and higher feed pressure to increase CO conversion. **Figure 3**

shows the results of WGS reaction in CCDP membrane reactor without catalyst with $SV=150\text{ h}^{-1}$ at two different temperatures as a function of feed pressure. At 1 bar and between 800 and 850 °C, the CO conversion and CO_2 recovery increase from 65 to 70% and 9 to 19%, respectively. Thermodynamically, the CO conversion decreases with temperature for the WGS reaction, as shown by the equilibrium conversion at 800 and 850 °C in **Figure 3a**. However, CO_2 removal by the CCDP membrane shifts the reaction equilibrium towards the products, enhancing the CO conversion. The CO conversion for the WGS reaction in the catalyst-free CCDP reactor reported here is much higher than we previously reported [17] as a result of different operating conditions.

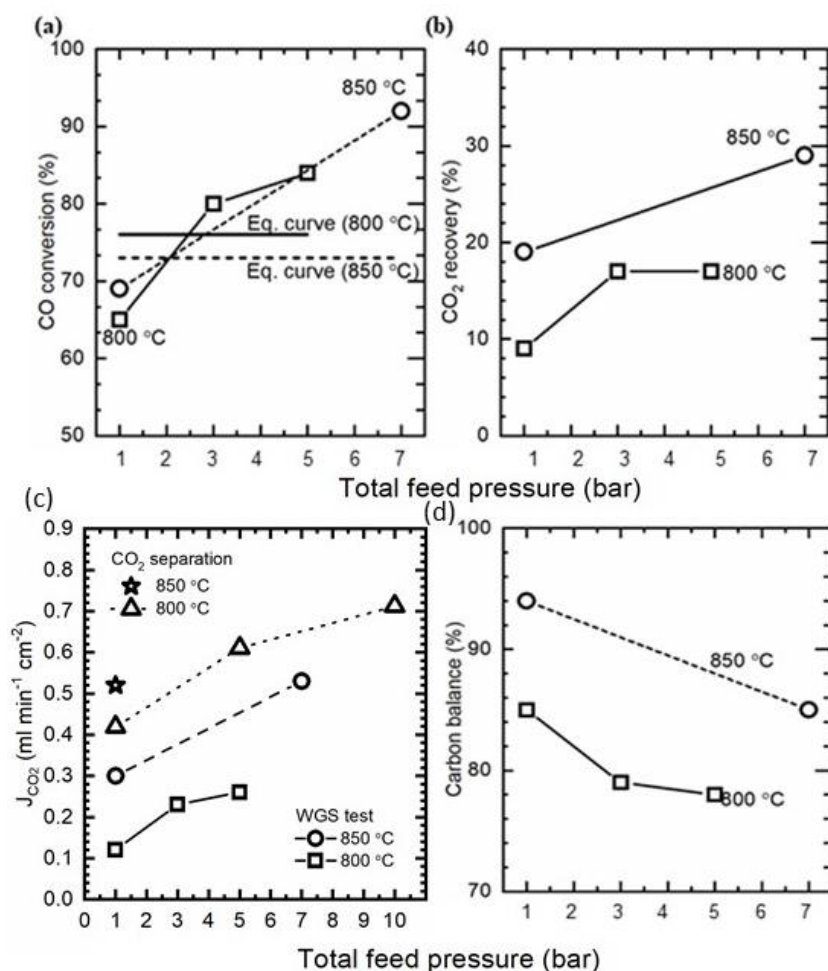


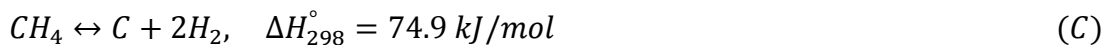
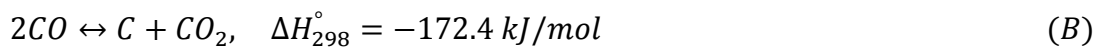
Figure 3. Results of WGS reaction performance without catalyst in SDC-carbonate membrane reactor and $SV=150\text{ h}^{-1}$ at 800 and 850 °C as a function of total feed pressure: (a) CO conversion

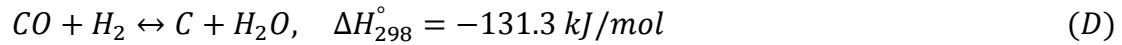
in the membrane reactor, (b) CO₂ recovery in the membrane reactor, (c) CO₂ permeation flux for WGS reaction in membrane reactor in comparison with CO₂ separation with equal molar CO₂:N₂ feed, (d) carbon balance in the membrane reactor.

Figure 3b shows that CO₂ recovery increases with the total feed pressure due to the increased CO₂ permeation flux driven by a higher CO₂ partial pressure on the reaction side [24,25]. This effect also promotes the shifting of the WGS reaction equilibrium and increases the CO conversion, as shown by reaction (A). However, under such space-velocity, carbon balance is less than 100%, between 77% and 95%, indicating that WGS is accompanied by a significant amount of side reactions.

Figure 3c shows CO₂ permeation flux in the membrane reactor with WGS reaction feed. The CO₂ permeation flux increases with feed pressure and reactor temperature due to a strong temperature dependence of ionic conductivity of the two phases in the membranes and increases in driving force due to increased feed pressure. However, CO₂ permeation fluxes with WGS reaction are lower than with equal-molar CO₂:N₂ feed without WGS reaction. This is because, in the separation experiments, the CO₂ partial pressure is 50% of the total-feed pressure, much larger than the average CO₂ partial pressure in the reaction stream for WGS according (the initial CO₂ partial pressure is about 5% of the total feed pressure (feed composition: 45.7:13.1:41.3:182.8 for CO/CO₂/N₂/steam). The driving force for CO₂ permeation through the dual-phase membrane in the WGS reaction is lower than that in CO₂ separation.

Figure 3d shows carbon balance decreases as pressure increases or temperature decreases. It is well known that the WGS reaction at high temperatures is accompanied by the formation of carbon through the following reactions [26,28]:





Reaction (B) is a CO disproportionation known as the Boudouard reaction. Reaction (C) is CH₄ decomposition, but it is unlikely in the present study because our experimental results show no CH₄ formation through CO/CO₂ methanation. Reactions (D) and (E) are CO and CO₂ hydrogenation, which may occur in this work. All reactions (B), (D), and (E) are exothermic and gas-volume-reduction reactions. Thus thermodynamically, the formation of carbon is favored at lower temperatures and high pressures. This explains the temperature and pressure dependence of carbon balance shown in **Figure 3d**.

Experiments of WGS reaction in the membrane reactor without catalyst were performed at low space velocities for higher CO conversion and CO₂ recovery, as was demonstrated in our modeling study [25]. However, carbon yield from the side reactions also increases with decreasing space velocity. Increasing the space velocity may lower the side reaction, but it also reduces the CO conversion in the WGS reaction in the catalyst-free membrane reactor. To address the carbon formation issue, one could try to improve the kinetic rate of the WGS reaction using a catalyst. This way, it is possible to perform a WGS reaction with sufficiently high CO conversion at a high space velocity that minimizes carbon yield.

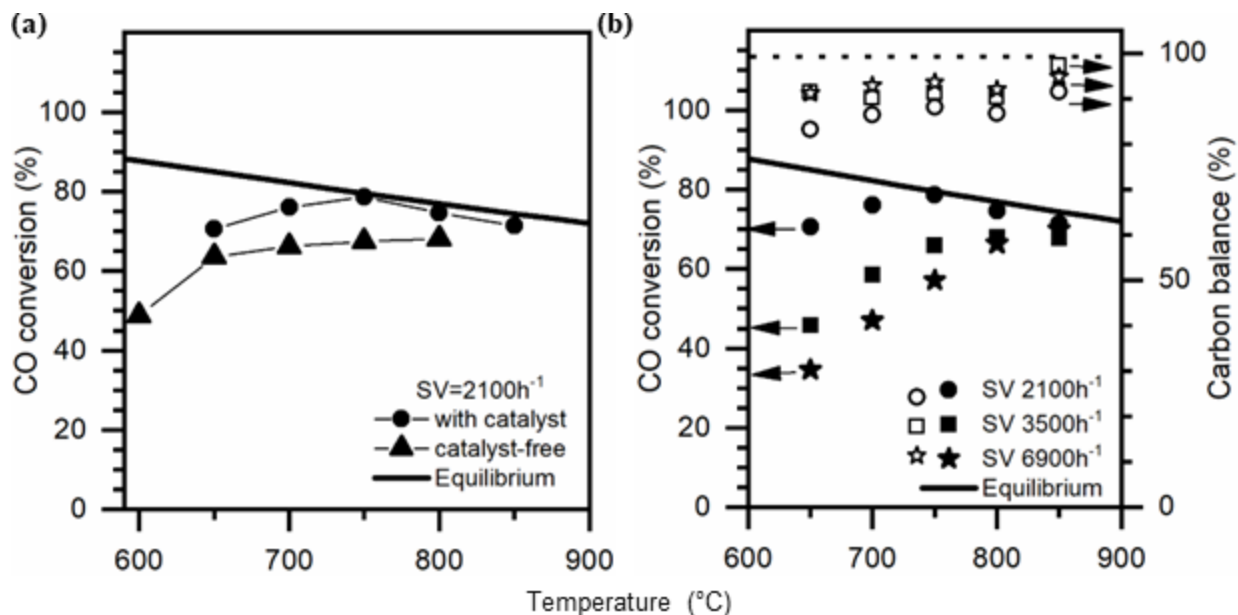


Figure 4. WGS reaction results in a fixed-bed reactor with a catalyst at 10 bar: (a) performance comparison with the results without catalyst (both cases at $SV=2100\text{ h}^{-1}$), and (b) performance at different space velocities as a function of temperature.

To confirm the high-temperature catalytic activity, **Figure 4a** compares WGS reaction results in a fixed-bed reactor with and without catalyst at 10 bar. With catalyst at $SV=2100\text{ h}^{-1}$, the reaction rate and hence CO conversion increases with temperature and reaches the equilibrium at 750 °C and then decreases with temperature following the equilibrium conversion data. But without a catalyst, at the same space velocity, the conversion of WGS, though also increasing with temperature, does not reach the equilibrium in the entire range of operating temperature. The comparison clearly shows that the catalyst used in this work effectively enhances the WGS reaction rate.

Figure 4b shows the CO conversion and carbon balance for WGS in a fixed-bed reactor with the catalyst at different space velocities as a function of temperature. As expected, the CO conversion decreases with increasing space velocity. For the two data at higher space velocity, the CO conversion increases with temperature but barely reaches the equilibrium at 850 °C. The carbon balance at the whole space velocity range increases with temperature, reflecting the

decreasing carbon yield for the exothermic side reactions as temperature increases. At 850 °C, the carbon balance is over 90%, and it is essentially 100% at the higher space velocity. However, at a space velocity higher than 2100 h⁻¹, the CO conversion of WGS is lower. These results help select the operating conditions for WGS reaction with the catalyst in the membrane reactor, as shown next.

On the one hand, the minimization of the formation of carbon with a carbon balance higher than 90% in a catalyst-free membrane reactor for WGS reaction is achieved at 850 °C and a pressure lower than 7 bar. In the catalyzed fixed-bed reactor, it can be reached at space velocities as high as 2100 h⁻¹ and 700 °C. On the other hand, CO conversion higher than 90% can be achieved at 850 °C, 7 bar, and SV=150 h⁻¹. Combining the results of both experiments one can define optimal reaction conditions, the operating conditions of 850 °C, 7 bar, S/C=4, and SV ~2100 h⁻¹ allowed us to establish the optimized WGS reaction with a catalyst in the membrane reactor.

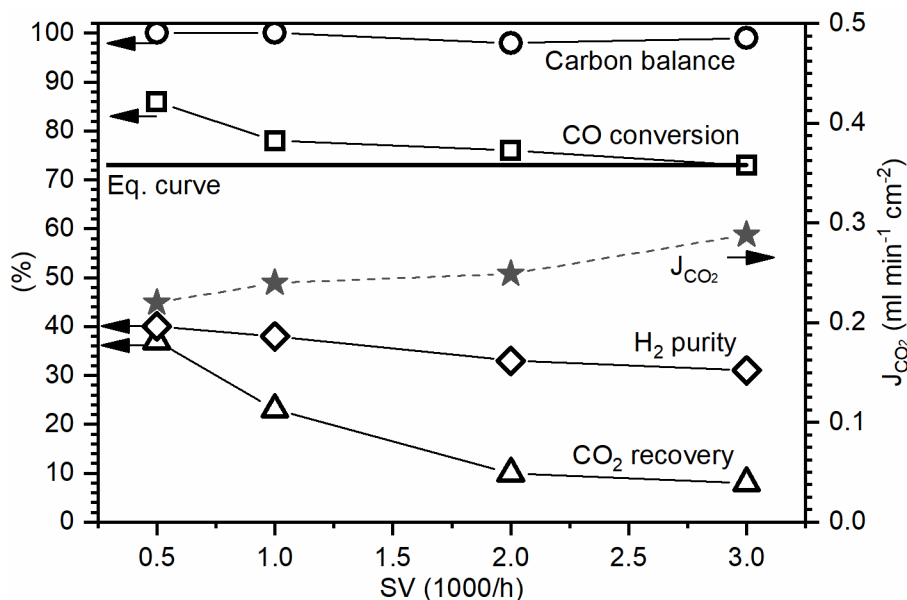


Figure 5. WGS reaction in SDC-carbonate membrane reactor with a catalyst at 850 °C, 7 bar, and S/C=4 as different space velocity

Figure 5 shows the experimental results of the WGS reaction with a catalyst in the membrane reactor as a function of space velocity at 850 °C, 7 bar, and S/C=4. CO conversion and CO₂ recovery decrease with the space velocity, and no carbon deposition is observed in the whole space velocity range because the carbon balance reaches 100% at SV > 500 h⁻¹. The CO₂ permeation through the membrane helps enhance the CO conversion at SV < 2000 h⁻¹, in which the CO conversion is larger than the equilibrium. For instance, the CO₂ removal increases the CO conversion to 87%, 14% over the equilibrium conversion at SV = 500 h⁻¹. The CO₂ permeation flux increases, and CO₂ recovery decreases with increasing space velocity. This is because as space velocity increases CO₂ formation rate (not conversion) increases more than the CO₂ removal rate, resulting in an increase in the average CO₂ partial pressure on the reactor side. For example, the CO₂ concentration in the retentate of on the feed side increases from 26 to 32% as space velocity increases from 500 to 3000 h⁻¹. Higher CO₂ concentration produces a larger driving force for CO₂ permeation flux. This also explains decreasing CO₂ recovery with increasing SV. These results are consistent with our previous modeling study [25]. Dry-based H₂ purity decreases with increasing SV because the CO conversion and the CO₂ removal decrease at higher SV. H₂ purity is lower than 40% because the dry composition of the feed gas contains a high concentration of N₂, ~41.3%.

Figures 6 and **7** present the characterization results of the SDC-carbonate membrane used in the membrane reactor before and after the WGS reaction test with and without catalyst at 850 °C and total feed pressure of 7 bar. **Figure 6** gives optical photographs (**a1**, **a2**, **a3**) and SEM micrographs (**b1**, **b2**, **b3**) of the outer surface of the fresh SDC-carbonate membrane and the SDC-carbonate membrane after the WGS reaction test without catalyst and with catalyst.

The optical micrographs show that the membrane surface changed in color after the WGS reaction test. Before the test, the membrane has a typical light yellow color of the SDC phase. After the catalyst-free test, the membrane surface exhibits gray stains, but the membrane surface remains light yellow after the test with catalyst. In the first case, the gray stains are attributed to the products of the side reaction deposited on the membrane surface.

Also, SEM micrographs show microstructural differences on the outer surface of the membranes. SDC-carbonate membrane before the test shows a dense surface with uniform distribution of SDC and carbonate phases, with the bright spots being the SDC phase and dark areas the carbonate phase. Also, SDC has a narrow particle size distribution with an average particle size between 100 and 200 nm (**Figure 6-b1**). However, the SDC-carbonate membrane after the catalyst-free WGS reaction test shows larger bright agglomerates of 2-3 μm (**Figure 6-b2**), ascribed to the products of the side reactions deposited on the membrane, as it is discussed in the next paragraph.

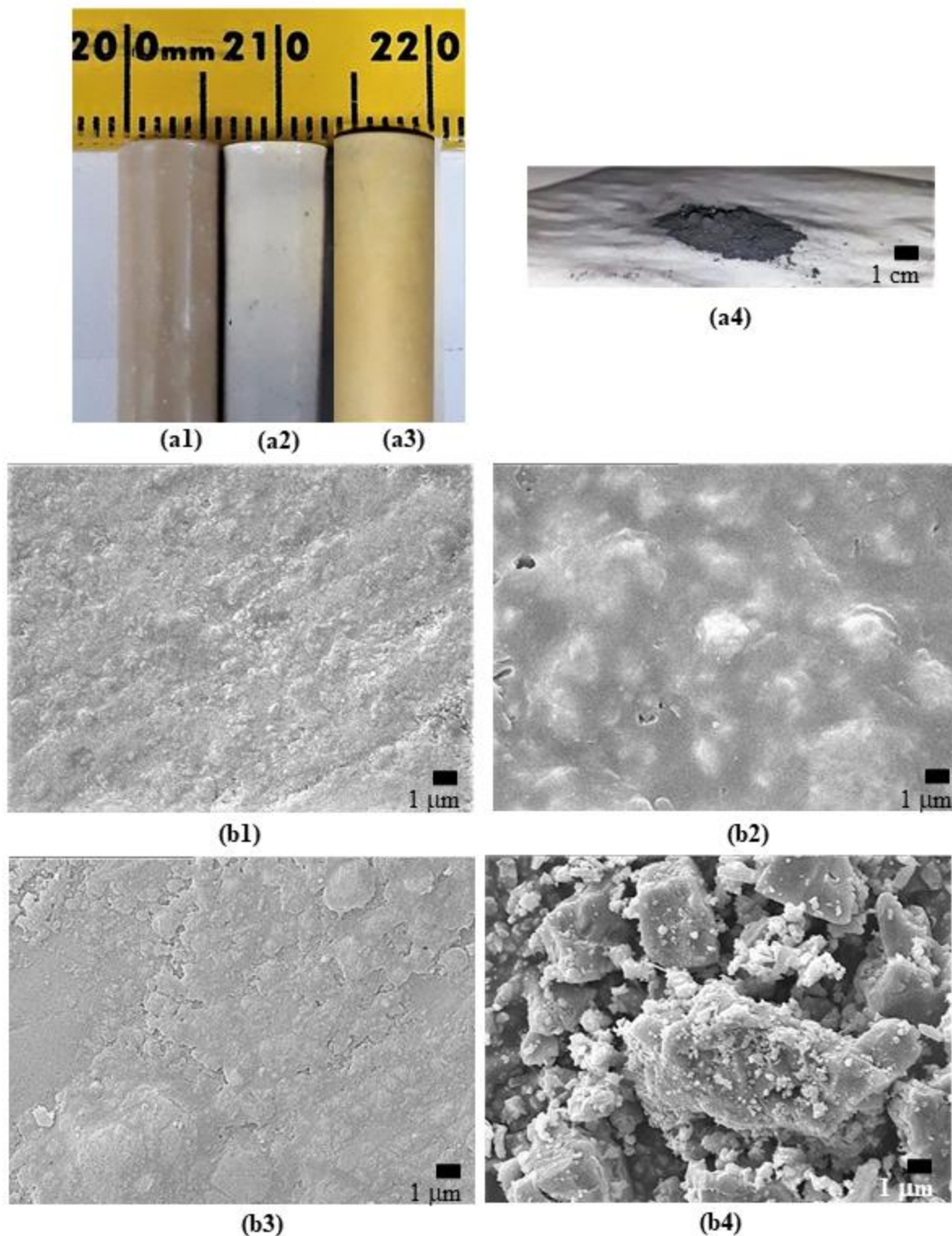


Figure 6. Optical photographs and SEM images of the surface of the SDC-carbonate membrane before the test (a1) and (b1), after catalyst-free test (a2) and (b2), and after the test with catalyst (a3) and (b3). Picture and SEM image of black powder removed from the wall of the steel module after the catalyst-free test (a4) and (b4).

After the test with the catalyst, the surface presents smaller particles (**Figures 6-b3**) similar to SDC-carbonate before the test. SEM images show that both membranes remain dense after the WGS reaction test. The MC can resist high feed pressures because, according to the Young-Laplace equation, the SDC support with 190 nm pores can produce enough capillary force for the MC to resist a maximum transmembrane pressure of 47 atm [24]. Also, the gas-tight membrane after the test for 8 h was proved by the unsteady-state helium permeance at room temperature, where the helium permeance was of the order of $10^{-11} \text{ mol}\cdot\text{s}^{-1}\cdot\text{m}^{-2}\cdot\text{Pa}^{-1}$.

The optical photograph and SEM micrograph of the black powder removed from the inner wall of the membrane reactor module after the catalyst-free WGS reaction test is given in **Figure 6 (a4) and (b4)**. This powder comprises agglomerates between 0.5 and 7 μm . These agglomerates were also deposited on the surface of the membrane after the WGS reaction without the catalyst, as can be observed by comparing the SEM images of the SDC-carbonate membrane (**Figure 6-b2**) and the black powder (**Figure 6-b4**) after the catalyst-free WGS test. SDC-carbonate membrane surface after the test with catalyst has no agglomerates, attributed to the minimized side reaction. Optical and SEM images confirm the deposition of products from side reactions on the membrane surface of the catalyst-free MR, and the membrane remains dense after the WGS reaction test on catalyst and catalyst-free MR.

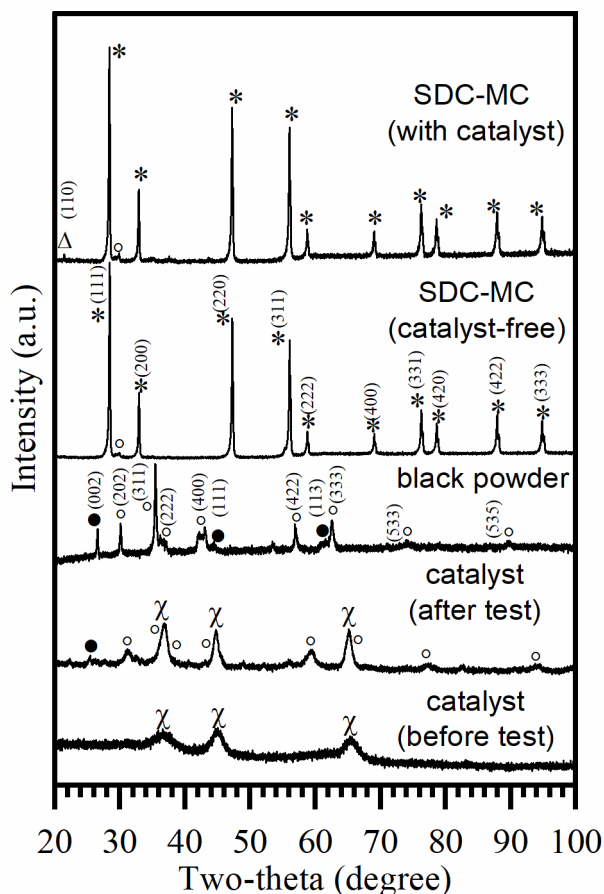


Figure 7. XRD pattern of SDC-carbonate membrane after WGS reaction test with and without catalyst, black powder removed from the wall of the module after the catalyst-free test, and catalyst after and before the WGS reaction test. (*) SDC, (Δ) lithium carbonate, (•) Graphite, (°) Fe_3O_4 , and (χ) High-temperature Mo-Co-based catalyst.

Figure 7 presents the XRD patterns of the SDC-carbonate membrane surface after the WGS reaction test with and without catalyst, the black powder produced by side reactions, and the catalyst before and after the reaction test. The outer surface of the SDC-carbonate membrane after the catalyst-free WGS test shows the crystalline structure of the SDC phase and a secondary phase at 31° . After this experiment, the removed black powder (**Figure 6 (b4)**) from the module was analyzed by XRD. This powder was identified as a mixture of graphite (C, COD # 96-901-2231) and magnetite with a cubic system and cell parameter of 8.39 \AA (Fe_3O_4 , COD #

96-900-39770). The secondary phase on the SDC-carbonate membrane at 31° corresponds to magnetite deposited on the membrane surface. The diffraction peaks of the graphite are not observed in the XRD pattern because the intensity of these peaks is indistinguishable due to their low weight percent on the surface of the membrane. The Boudouard reaction produced carbon, and the Fe_3O_4 was formed due to the interface reactions on the Fe-rich steel module surface with the feed gas, which is also promoted at high pressures [32]. These results confirm the chemical stability of the membrane after the WGS reaction without a catalyst because the SDC crystalline structure remains stable, and no secondary phases made of cerium or samarium were detected.

Concerning the surface of the SDC-carbonate membrane after the test with catalyst, the XRD pattern shows the crystalline structure of the SDC phase, the lithium carbonate phase (COD #96-900-9642), at 22.33° , and the magnetite, at 31° , with a cubic system and cell parameter of 8.12 \AA (COD #96-900-2331). The diffraction peaks of this magnetite are slightly shifted to larger angles with respect to the magnetite observed in the catalyst-free test. The catalyst before the test exhibits a typical XRD profile of a nanometric microstructure with large peak broadening. After the test, the XRD peaks of the catalyst are narrower than before the test, which means that the particle size of the catalyst slightly increased after the high-temperature test. However, the catalyst was chemically stable as confirmed by no change in the crystalline structure after the test. Also, analysis of the diffraction peaks of the magnetite gives a cell parameter of 8.12 \AA , but XRD peaks of carbon are not presented in the catalyst. The XRD analysis of the SDC-carbonate membrane after the WGS reaction test with and without catalyst shows that the crystalline structure of the SDC-carbonate membrane was not affected by the presence of other crystalline phases formed by side reactions. In both cases, the membranes are stable under WGS reaction conditions, at least during the 8 hr of the test at 850°C and 7 bar.

Conclusions

CO₂-permeable samarium-doped ceria and molten-carbonate membrane reactors effectively enhance water-gas shift reaction with simultaneous CO₂ capture, even under catalyst-free conditions at high temperatures and pressures. The catalyst-free membrane reactor can achieve CO conversion higher than 90%, 20% over the equilibrium conversion, with 29% CO₂ recovery at 850 °C, 7 bar, S/C=4, and low SV of 150 h⁻¹, accompanied by a significant amount of unwanted side reaction of carbon formation. The membrane reactor with a high-temperature water-gas shift catalyst shows enhanced performance for water-gas shift reaction and CO₂ recovery with complete elimination of carbon deposition at the same operating pressure and temperature but higher space velocity (>500 h⁻¹). The ceramic-carbonate membranes are chemically stable under the water-gas shift experiment conditions and remain gas-tight and dense after high pressures and temperatures.

Acknowledgments

The authors would like to acknowledge the support of the Department of Energy (DOE) (DE-FE0031634) for this study. O.O.E. acknowledges the support from a CONACYT scholarship for postdoctoral research. We acknowledge the use of facilities within the Eyring Materials Center at Arizona State University, supported in part by NNCI-ECCS-1542160.

References

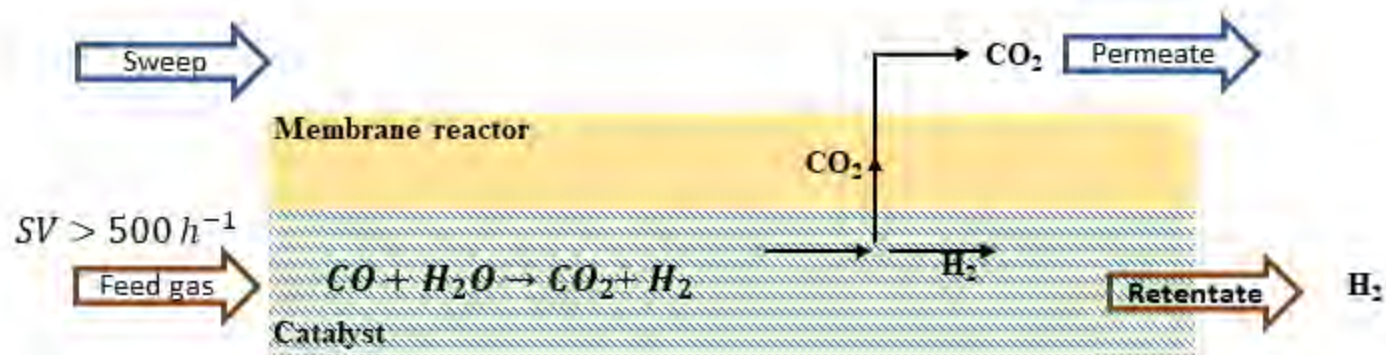
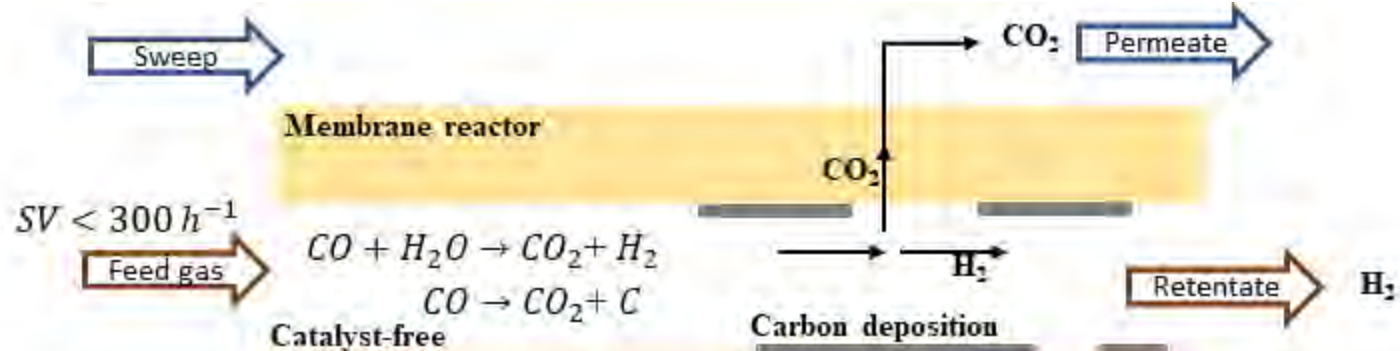
- [1] C.C. Cormos, Integrated assessment of IGCC power generation technology with carbon capture and storage (CCS), *Energy*. 42 (2012) 434–445. <https://doi.org/10.1016/j.energy.2012.03.025>.
- [2] S. Ferguson, G. Skinner, J. Schiekea, K.C. Leeb, E. Van Dorstb, High efficiency integrated gasification combined cycle with carbon capture via technology advancements and improved heat integration, *Energy Procedia*. 37 (2013) 2245–2255.

- <https://doi.org/10.1016/j.egypro.2013.06.105>.
- [3] B. Smith R J, M. Loganathan, M.S. Shantha, A review of the water gas shift reaction kinetics, *Int. J. Chem. React. Eng.* 8 (2010). <https://doi.org/10.2202/1542-6580.2238>.
- [4] Y.L. Lee, K. Lee, C. Hyun Ko, H.S. Roh, Optimization of nano-catalysts for application in compact reformers, *Chem. Eng. J.* 431 (2022) 134299. <https://doi.org/10.1016/j.cej.2021.134299>.
- [5] M.A. Soria, C. Rocha, S. Tosti, A. Mendes, L.M. Madeira, CO_x free hydrogen production through water-gas shift reaction in different hybrid multifunctional reactors, *Chem. Eng. J.* 356 (2019) 727–736. <https://doi.org/10.1016/j.cej.2018.09.044>.
- [6] W.-H. Chen, C.-Y. Chen, Water gas shift reaction for hydrogen production and carbon dioxide capture: A review, *Appl. Energy.* 258 (2020) 114078. <https://doi.org/10.1016/j.apenergy.2019.114078>.
- [7] K.R. Hwang, S.W. Lee, S.K. Ryi, D.K. Kim, T.H. Kim, J.S. Park, Water-gas shift reaction in a plate-type Pd-membrane reactor over a nickel metal catalyst, *Fuel Process. Technol.* 106 (2013) 133–140. <https://doi.org/10.1016/j.fuproc.2012.07.013>.
- [8] A. Brunetti, A. Caravella, E. Fernandez, D.A. Pacheco Tanaka, F. Gallucci, E. Drioli, E. Curcio, J.L. Viviente, G. Barbieri, Syngas upgrading in a membrane reactor with thin Pd-alloy supported membrane, *Int. J. Hydrogen Energy.* 40 (2015) 10883–10893. <https://doi.org/10.1016/j.ijhydene.2015.07.002>.
- [9] S. Pati, A. Jangam, Z. Wang, N. Dewangan, M.H. Wai, S. Kawi, Catalytic Pd_{0.77}Ag_{0.23} alloy membrane reactor for high temperature water-gas shift reaction: Methane suppression, *Chem. Eng. J.* 362 (2019) 116–125. <https://doi.org/10.1016/j.cej.2018.12.112>.
- [10] S. Araki, H. Miyanishi, H. Yano, S. Tanaka, Y. Miyake, Water Gas Shift Reaction in a Membrane Reactor Using a High Hydrogen Permselective Silica Membrane, *Sep. Sci. Technol.* 48 (2013) 76–83.
- [11] A. Brunetti, G. Barbieri, E. Drioli, T. Granato, K. Lee, A porous stainless steel supported silica membrane for WGS reaction in a catalytic membrane reactor, *Chem. Eng. Sci.* 62 (2007) 5621–5626. <https://doi.org/10.1016/j.ces.2007.01.054>.
- [12] R. Nishida, T. Tago, T. Saitoh, M. Seshimo, S. Nakao, Development of CVD silica membranes having high hydrogen permeance and steam durability and a membrane reactor for a water gas shift reaction, *Membranes (Basel).* 9 (2019) 139–150.
- [13] S.J. Kim, S. Yang, G.K. Reddy, P. Smirniotis, J. Dong, Zeolite membrane reactor for high-temperature water-gas shift reaction: Effects of membrane properties and operating conditions, in: *Energy and Fuels*, 2013. <https://doi.org/10.1021/ef302014n>.
- [14] X. Dong, H. Wang, Z. Rui, Y.S. Lin, Tubular dual-layer MFI zeolite membrane reactor for hydrogen production via the WGS reaction: Experimental and modeling studies, *Chem. Eng. J.* 268 (2015) 219–229. <https://doi.org/10.1016/j.cej.2015.01.046>.
- [15] I.G.B.N. Makertihartha, M. Zunita, Z. Rizki, P.T. Dharmawijaya, Advances of zeolite

- based membrane for hydrogen production via water gas shift reaction, *J. Phys. Conf. Ser. Pap.* 877 (2017) 012076. <https://doi.org/10.1088/1742-6596/877/1/012076>.
- [16] H. Yin, J. Shang, J. Choi, A.C.K. Yip, Generation and extraction of hydrogen from low-temperature water-gas-shift reaction by a ZIF-8-based membrane reactor, *Microporous Mesoporous Mater.* 280 (2019) 347–356. <https://doi.org/10.1016/j.micromeso.2019.02.030>.
- [17] X. Dong, Y.S. Lin, Catalyst-free ceramic-carbonate dual phase membrane reactor for hydrogen production from gasifier syngas, *J. Memb. Sci.* 520 (2016) 907–913. <https://doi.org/10.1016/j.memsci.2016.08.036>.
- [18] S. Sun, Y. Wen, K. Huang, A new ceramic-carbonate dual-phase membrane for high-flux CO₂ capture, *ACS Sustain. Chem. Eng.* 9 (2021) 5454–5460. <https://doi.org/10.1021/acssuschemeng.1c00860>.
- [19] T. Chen, Z. Wang, J. Hu, M.H. Wai, S. Kawi, Y.S. Lin, High CO₂ permeability of ceramic-carbonate dual-phase hollow fiber membrane at medium-high temperature, *J. Memb. Sci.* 597 (2020) 117770. <https://doi.org/10.1016/j.memsci.2019.117770>.
- [20] D. González-Varela, O. Ovalle-Encinia, J.F. Gómez-García, G. Tavizon, H. Pfeiffer, High-temperature CO₂ perm-selectivity of yttrium-doped SDC ceramic-carbonate dual-phase membranes, *React. Chem. Eng.* 6 (2021) 321–334. <https://doi.org/10.1039/d0re00375a>.
- [21] J.A. Fabián-Anguiano, R. Ortega-Lugo, M.J. Ramírez-Moreno, B. Zeifert, C. Gómez-Yáñez, J. Ortiz-Landeros, Concurrent and modulated separation of CO₂ and O₂ by a fluorite/perovskite-based membrane, *Int. J. Appl. Ceram. Technol.* 18 (2021) 1307–1320. <https://doi.org/10.1111/ijac.13739>.
- [22] H. Wu, G. Nile, J.Y.S. Lin, Mixed-conducting ceramic-carbonate dual-phase membranes: Gas permeation and counter-permeation, *J. Mem.* 605 (2020) 118093. <https://doi.org/10.1016/j.memsci.2020.118093>.
- [23] S. Afzal, A. Khan, Recent advances in molten-carbonate membranes for carbon dioxide separation: Focus on material selection, geometry, and surface modification, *Sci. World J.* 2021 (2021). <https://doi.org/10.1155/2021/1876875>.
- [24] O. Ovalle-Encinia, J.Y.S. Lin, High-pressure CO₂ permeation properties and stability of ceramic-carbonate dual-phase membranes, *J. Memb. Sci.* 646 (2022) 120249. <https://doi.org/10.1016/j.memsci.2021.120249>.
- [25] L. Meng, O. Ovalle-Encinia, J.Y.S. Lin, Catalyst-free ceramic-carbonate dual-phase membrane reactors for high-temperature water gas shift: A simulation study, *Ind. Eng. Chem. Res.* 60 (2021) 3581–3588. <https://doi.org/10.1021/acs.iecr.1c00541>.
- [26] R.-Y. Chein, C.-T. Yu, Thermodynamic equilibrium analysis of water-gas shift reaction using syngases-effect of CO₂ and H₂S contents, 141 (2017) 1004–1018. <https://doi.org/10.1016/j.energy.2017.09.133>.
- [27] J. Shin, M.S. Kang, J. Hwang, Effects of bio-syngas CO₂ concentration on water-gas shift and side reactions with Fe-Cr based catalyst, *Int. J. Energy Res.* 45 (2021) 1857–1866.

<https://doi.org/10.1002/er.5861>.

- [28] D.L. Trimm, Coke formation and minimisation during steam reforming reactions, *Catal. Today*. 37 (1997) 233–238. [https://doi.org/10.1016/S0920-5861\(97\)00014-X](https://doi.org/10.1016/S0920-5861(97)00014-X).
- [29] F. Bustamante, R.M. Enick, R.P. Killmeyer, B.H. Howard, K.S. Rothenberger, A. V. Cugini, B.D. Morreale, M. V. Ciocco, Uncatalyzed and wall-catalyzed forward water-gas shift reaction kinetics, *AIChE J.* 51 (2005) 1440–1454. <https://doi.org/10.1002/aic.10396>.
- [30] K.G. Harry, A. Johnson, A non-destructive technique for measuring ceramic porosity using liquid nitrogen, *J. Archaeol. Sci.* 31 (2004) 1567–1575. <https://doi.org/10.1016/j.jas.2004.03.020>.
- [31] J. Ortiz-Landeros, T. Norton, Y.S. Lin, Effects of support pore structure on carbon dioxide permeation of ceramic-carbonate dual-phase membranes, *Chem. Eng. Sci.* 104 (2013) 891–898. <https://doi.org/10.1016/j.ces.2013.09.027>.
- [32] M.H.S. Bidabadi, S. Chandra-ambhorn, A. Rehman, Y. Zheng, C. Zhang, H. Chen, Z.-G. Yang, Carbon depositions within the oxide scale and its effect on the oxidation behavior of low alloy steel in low (0.1 MPa), sub-(5 MPa) and supercritical (10 MPa) CO₂ at 550°C, *Corros. Sci.* 177 (2020) 108950. <https://doi.org/10.1016/j.corsci.2020.108950>.



$$P_{feed} - P_{permeate} > 7 \text{ atm}$$